



A Journal of the Gesellschaft Deutscher Chemiker

Angewandte Chemie

GDCh

International Edition

www.angewandte.org

Accepted Article

Title: Electric-Field Mediated Electron Tunneling of Supramolecular Naphthalimide Nanostructures for Biomimetic H₂ Production

Authors: Jinlin Long, Huan Lin, Zhiyun Ma, Jiwu Zhao, Yang Liu, Jinquan Chen, Junhui Wang, Kaifeng Wu, Huaping Jia, Xuming Zhang, Xinhua Cao, Xuxu Wang, and Xianzhi Fu

This manuscript has been accepted after peer review and appears as an Accepted Article online prior to editing, proofing, and formal publication of the final Version of Record (VoR). This work is currently citable by using the Digital Object Identifier (DOI) given below. The VoR will be published online in Early View as soon as possible and may be different to this Accepted Article as a result of editing. Readers should obtain the VoR from the journal website shown below when it is published to ensure accuracy of information. The authors are responsible for the content of this Accepted Article.

To be cited as: *Angew. Chem. Int. Ed.* 10.1002/anie.202009267

Link to VoR: <https://doi.org/10.1002/anie.202009267>

RESEARCH ARTICLE

Electric-Field Mediated Electron Tunneling of Supramolecular Naphthalimide Nanostructures for Biomimetic H₂ Production

Huan Lin,^{*,[a,b]} Zhiyun Ma,^{*,[a]} Jiwu Zhao,^[a] Yang Liu,^[a] Jinqun Chen,^[c] Junhui Wang,^[d] Kaifeng Wu,^[d] Huaping Jia,^[e] Xuming Zhang,^[e] Xinhua Cao,^[f] Xuxu Wang,^[a] Xianzhi Fu,^[a] and Jinlin Long^{*,[a]}

*These authors contributed equally to this work.

- [a] Dr. H. Huan, Ms Z. Ma, Dr. J. Zhao, Ms Y. Liu, Prof. X. Wang, Prof. X. Fu, Prof. J. Long
Department State Key Laboratory of Photocatalysis on Energy and Environment Institution, College of Chemistry
Fuzhou University, Fuzhou 350108, P. R. China
E-mail: jilong@fzu.edu.cn
- [b] Dr. H. Huan
College of Chemical Engineering
Fuzhou University, Fuzhou 350108, P. R. China
- [c] Prof. J. Chen
Department State Key Laboratory of Precision Spectroscopy, Zhongshan Campus
East China Normal University, Shanghai 200062, P. R. China
- [d] Prof. J. Wang, Prof. K. Wu
State Key Laboratory of Molecular Reaction Dynamics and Dynamics Research Center for Energy and Environmental Materials
Dalian Institute of Chemical Physics, Chinese Academy of Science, Dalian 116023, P. R. China
- [e] Dr H. Jia, Prof. X. Zhang
Department of Applied Physics
The Hong Kong Polytechnic University, Hong Kong 999077, P. R. China
- [f] Prof. X. Cao
College of Chemistry and Chemical Engineering
Xinyang Normal University, Xinyang 464000, P.R. China

Abstract: This work reported on the smart design and synthesis of two novel semiconducting *bis* (4-ethynyl-bridging 1, 8-naphthalimide) bolaamphiphiles (BENI-COO⁻ and BENI-NH₃⁺) to fabricate supramolecular metal-insulator-semiconductor (MIS) nanostructures for biomimetic hydrogen evolution under visible light irradiation. An impressive H₂ evolution rate of ca. 3.12 mmol·g⁻¹·h⁻¹ and an apparent quantum efficiency (AQE) of ca. 1.63 % at 400 nm were achieved over the BENI-COO⁻-NH₃⁺-Ni MIS photosystem prepared by electrostatic self-assembly of BENI-COO⁻ with the opposite-charged DuBois-Ni catalysts. The hot electrons of photoexcited BENI-COO⁻ nanofibers were tunnelled to the molecular Ni collectors across a salt bridge and an alkyl region of 2.2-2.5 nm length at a rate of 6.10×10⁸ s⁻¹, which is five-times larger than the BENI-NH₃⁺ nanoribbons (1.17×10⁸ s⁻¹). The transient spectral studies revealed that the electric field benefited significantly the electron tunneling dynamics and compensated the charge-separated states insufficient in the BENI-COO⁻ nanofibers, consequently a comparable hydrogen evolution rate to the inverse BENI-NH₃⁺-COO⁻-Ni photosystem.

Introduction

The creation of soft photoactive materials that integrate photoabsorbers, charge-transport and catalytic function components to make storable fuels is an intensely interesting target in the multidisciplinary domain of chemistry, materials and renewable energy. Tremendous effort has been devoted to developing π -conjugated organic polymers and crystalline covalent-organic frameworks (COFs) to fabricate artificial photosystems that can convert solar energy to a chemical form.^[1] Recently, one exceptional example is the perylene monoimide

(PMI) amphiphiles reported by Stupp and coworkers, who demonstrated for the first time that the supramolecular hydrogels formed by self-assembling PMI nanoribbons integrated a molecular catalyst into a soft fuel-generating material for the hydrogen evolution in the presence of a sacrificial agent, starting to further expand the availability of light-harvesting apparatuses in photosynthetic organisms.^[2] The extended multipolar π -system of this class of organic semiconductors with precisely-defined molecular formulas made it possible to fabricate numerous supramolecular architectures and nanostructures with novel and fascinating photophysical and photochemical properties. Therefore, the rational design of new molecular semiconductors with highly delocalized electronic structure is an exciting direction with great potential to achieve highly active next-generation artificial photosystems.

Many studies showed that the large exciton binding energy of organic semiconductors limited heavily the formation, separation and transport of charge-transfer excitons (CTEs) confined in nearest neighbor molecules,^[3] which are of most importance for the eventual applications for charge-induced reactions including hydrogen production, CO₂ reduction, and organic transformations, as a result, few kinds of organic semiconducting molecules were active for the photo-to-fuel conversion and photoredox catalysis.^[4] 1,8-naphthalimide (NI) and its derivatives are another attractive class of small-molecule organic semiconductors with extraordinary photo-, thermal, and chemical stability as well as excellent fluorescence quantum yields.^[5] The electron-deficient NI molecule can be functionalized at the N-imide site and aromatic core through an easy and cost-effective synthetic route. It allows to not only produce a vast array of NI derivatives, but also tune its photophysical and electronic properties.^[6] In addition, one of the predominant advantages is that the LUMO and HOMO levels of

RESEARCH ARTICLE

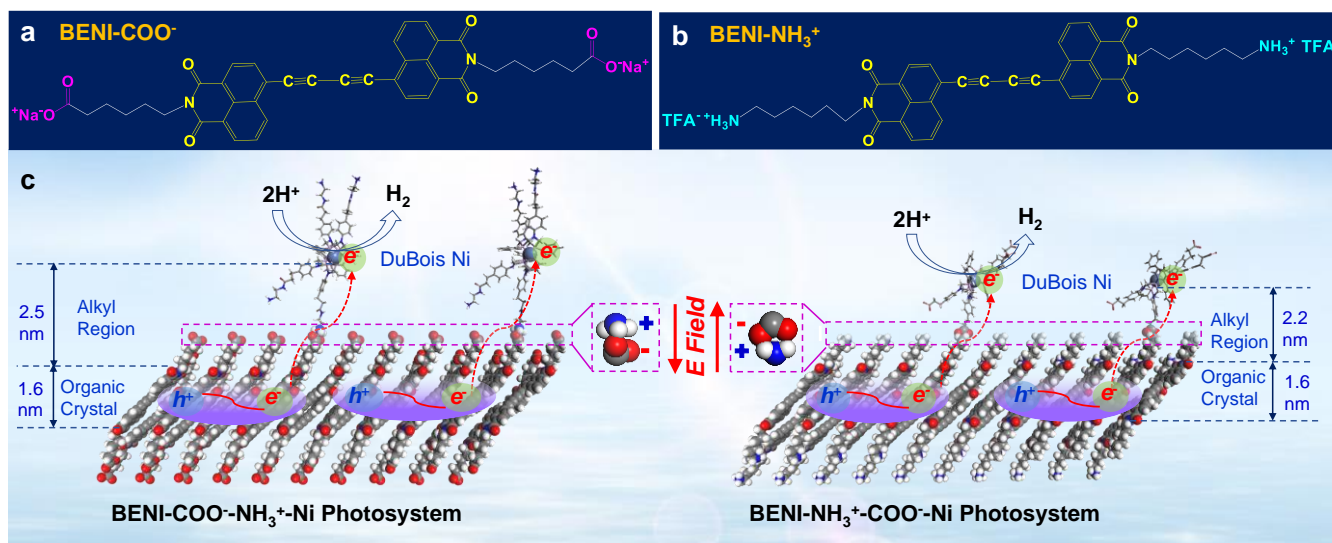


Figure 1. Molecular structure of BENI-COO⁻ (a) and BENI-NH₃⁺ (b). (c) Schematic illustration of the supramolecular semiconductor-insulator-metal (MIS) photosystems for biomimetic hydrogen production. The electric field formed by the salt bridges mediated the electron tunneling from the semiconducting BENI-based photoabsorbers to DuBois-Ni catalysts across a long-distance alkyl region.

the Ni derivatives spanned the redox potentials of H⁺/H₂ (0.00 V vs. RHE) and O₂/H₂O (+1.23 V vs. RHE),^[7] meaning the promising applications in photocatalytic water splitting. Given the UV-photo responsive characteristics of single Ni molecule, bridging two Ni molecules with ethynyl groups to extend the π -conjugated system to harvest visible photons and further facilitate migration of photogenerated excitons is the crucial consideration.^[8] Most importantly, introduction of polar, water-soluble groups into the parent Ni building blocks is a prerequisite for the target applications in aqueous media.^[9]

In this study, two water-soluble Ni-based molecular semiconductors, negative-charged *bis* (4-ethynyl-bridging (N-sodium hexanoate) 1,8-naphthalimide) (denoted as BENI-COO⁻, Figure 1a) and positive-charged *bis* (4-ethynyl bridging (N-hexylammonium trifluoroacetate) 1,8-naphthalimide) (denoted as BENI-NH₃⁺, Figure 1b) bolaamphiphiles, were designed smartly and synthesized successfully to construct a supramolecular photosystem of organic semiconductor-insulator-metal (MIS) nanostructures for efficient hydrogen evolution under visible light irradiation (Figure 1c). The heart of the supramolecular MIS-type photosystems is the organic chromophore of *bis* (4-ethynyl-bridging 1,8-naphthalimide) (BENI). It featured the symmetrical functionalization of two N atoms covalently bonded to long-chain aliphatic carboxylates or ammoniums. Not only the charged terminal groups imparted the high water-solubility to the BENI-based semiconductors, but also the specialized BENI building blocks can self-assemble into supramolecular nanostructures in aqueous media, such as nanoribbons or nanofibers. Two mimic enzymes, opposite-charged DuBois-Ni (Figure S1, See the Supporting Information) containing a bis (1,5-R'-diphospha-3,7-R''-diazacyclooctane) nickel (II) core,^[10] were served as the electron collectors for the catalytic reduction of protons into H₂. The atomic Ni sites are apart from the BENI chromophores across a long-distance alkyl region and a salt bridge interface at a distance of 2.2 nm for the BENI-NH₃⁺-COO⁻-Ni photosystem and 2.5 nm for the BENI-COO⁻-NH₃⁺-Ni photosystem (Figure 1c). The electron-transfer dynamics of the supramolecular MIS photosystems were studied in detail. It was found that the hot π -electrons of the photoexcited BENI nanostructures can be

efficiently separated and tunnelled to the atomic Ni sites to reduce protons to H₂. The electrostatic field (EF) formed in the salt bridges mediated significantly the electron tunneling dynamics and the hydrogen evolution rate.

Results and Discussion

Synthesis and self-assembly of BENI-COO⁻ and BENI-NH₃⁺.

The synthetic methodologies for the BENI-COO⁻ and BENI-NH₃⁺ bolaamphiphiles are described in the Experimental Procedures (see the Supporting Information for details). Owing to the strong π - π interaction between the BENI units, the two BENI-based bolaamphiphiles can be orderly stacked and self-assembled into aggregates with specific nanostructures. The density functional theory (DFT) simulation combined with the XRD data (Figure S2-4, See the Supporting Information) showed that the stacking was antiparallel and strongly displaced, leading to offset between the BENI units along their short and long axes in aggregates. The atomic force microscopy (AFM) results (Figure 2a) displayed that the self-assembled BENI-COO⁻ aggregates represented quasi-one-dimensional nanofibers with an ultrahigh aspect ratio of ca. 40 \pm 7 nm wide and several microns length. The height profile (Figure 2b) gave an average thickness of ca. 3.5 nm, approximately equal to the molecular length of BENI-COO⁻ (ca. 3.3 nm, Figure S2). This result indicated clearly that the π - π stacking is nearly perpendicular to the molecular plane,^[11] forming monolayer nanofibers, as shown in Figure 2d. The TEM image confirmed further the formation of the flat, fiber-like BENI-COO⁻ nanostructures (Figure 2c). Also, BENI-NH₃⁺ dissolved in water media was self-assembled to monolayer nanoribbons with an average thickness of ca. 3.0 nm (Figure 2e, f), in good agreement with the molecular length of BENI-NH₃⁺ (ca. 3.2 nm, Figure S3). One different point is that the BENI-NH₃⁺ nanoribbons are wider, about hundreds of nanometers (Figure 2g). It was mainly originated from the existence of additional H-bonds between the O atoms of naphthalimide units and the terminal ammonium groups of adjacent BENI-NH₃⁺ bolaamphiphiles (Figure S4, See

RESEARCH ARTICLE

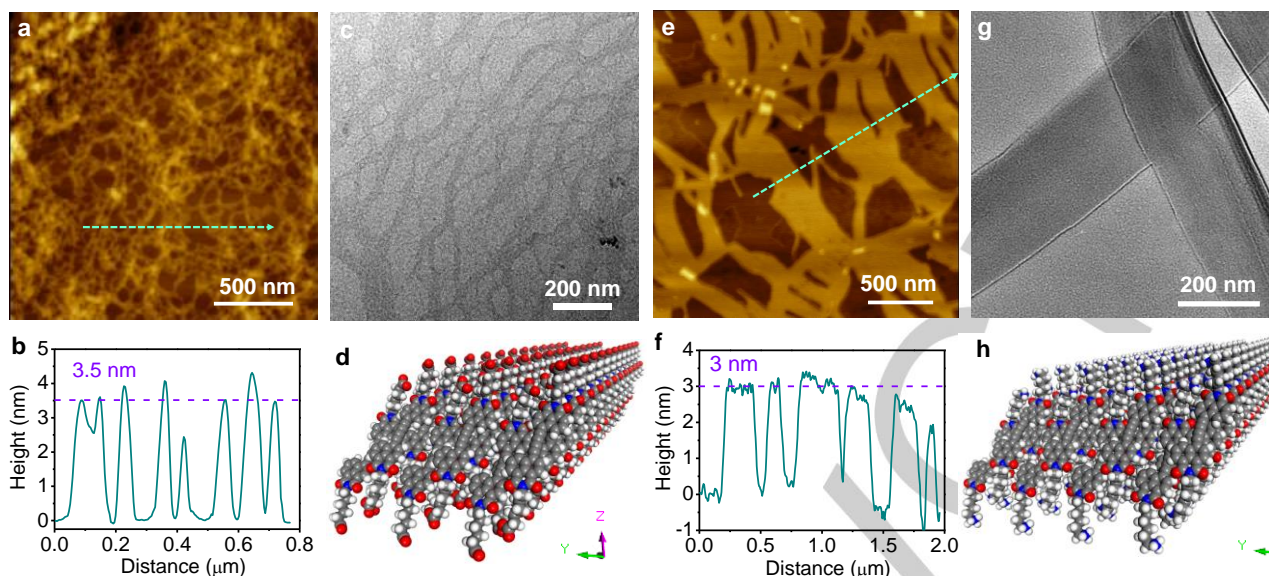


Figure 2. AFM images of the self-assembled BENI-COO⁻ aggregate (a) and BENI-NH₃⁺ aggregate (e). (b) and (f) Height profiles along the dashed green arrow in images a and e. TEM images of self-assembled BENI-COO⁻ aggregate (c) and BENI-NH₃⁺ aggregate (g). Schematic representation of the antiparallel and strongly-displaced packing of BENI-COO⁻ (d) and BENI-NH₃⁺ (h) bolaamphiphiles into a highly interdigitated monolayer to form supramolecular nanofiber and nanoribbon, respectively.

the Supporting Information), which led to the stronger intermolecular interaction along the short (y axis) dimension in comparison with the BENI-COO⁻ nanofibers (Figure 2h). This self-assembly will alter significantly the optical and photoexcitation properties of BENI-based molecular semiconductors.

Optical and photophysical properties of BENI-COO⁻ and BENI-NH₃⁺ bolaamphiphiles. Figure 3 represented the normalized steady-state absorption and fluorescence emission spectra of the BENI-based monomers and nanoaggregates, and the photophysical parameters were summarized in Table S1 (See the Supporting Information). Two BENI bolaamphiphiles dissolved in trifluoroethanol (TFE) have a predominant absorption at ca. 395 ± 3 nm (Figure 3a, 3b, black solid lines), which is assignable to the (0,1) π→π* transition of the BENI chromophore, and a lower-energy vibronic band at 423 ± 2 nm corresponding to the (0,0) π→π* transition of the BENI chromophore.^[12] Upon excitation, they emitted a strong fluorescence centered at 470 ± 5 nm with a shoulder at 445 ± 5 nm. The two fluorophores gave a high quantum yield (φ_F) of 59.4 % for BENI-COO⁻ and 55.5 % for BENI-NH₃⁺ (Figure 3a, 3b, black dashed lines). Significantly, the emission spectra attributed to transitions from the lowest single

excited states (S₁) appeared to be symmetrical approximately to the absorption spectra due to the mirror image rule.^[13] The S₁ lifetime was ca. 1.46 ± 1.0 ns (Figure 3c). These results showed that both of BENI-COO⁻ and BENI-NH₃⁺ bolaamphiphiles presented only in the form of monomeric molecules in TFE solutions.

After BENI-COO⁻ and BENI-NH₃⁺ were aggregated into nanostructures in H₂O, the two absorption bands were decreased in intensity, along with the slight broadening (Figure 3a-b, red solid lines). Notably, the (0, 0) transition band was red-shifted by 17 nm for BENI-COO⁻ and by 11 nm for BENI-NH₃⁺, and the (0, 1) transition band was also red-shifted by ca. 12 nm. The shift was mainly originated from the strong electronic coupling between adjacent chromophores, confirming further the predominance of J-type (slipped AA-stacked) packing modellings schemed in Figure 2d, 2h.^[14] Accordingly, the emission spectra of the BENI-COO⁻ and -NH₃⁺ nanostructures were changed greatly to be featureless (Figure 3a-b, red dashed lines). The main emission peak was broadened and redshifted to 525 nm for BENI-COO⁻ and to 530 nm for BENI-NH₃⁺, accompanied by the enormous decrease in intensity. The fluorescence decay kinetics can be

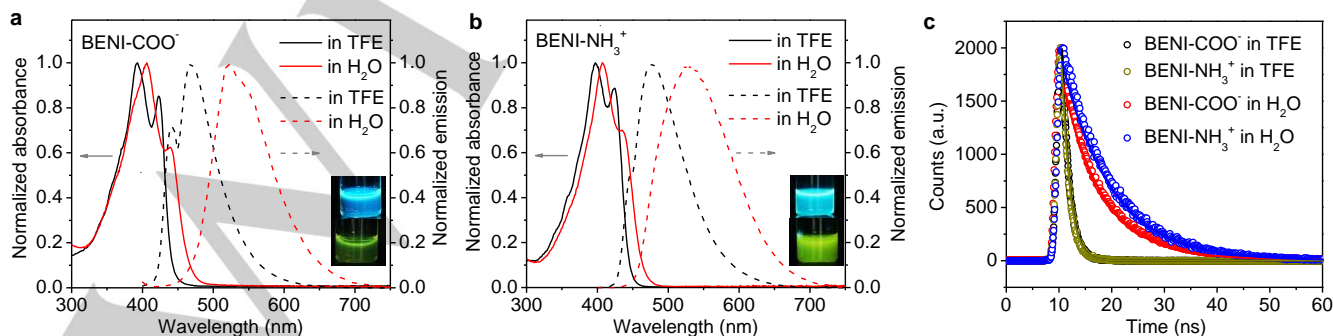


Figure 3. Normalized absorption (solid line) and fluorescence emission spectra (dashed line) of (a) BENI-COO⁻ and (b) BENI-NH₃⁺ (20 μM) in TFE (black) and H₂O (red), excited at 390 nm. Inset: the photographs of (a) BENI-COO⁻ (0.1 mM) and (b) BENI-NH₃⁺ (0.1 mM) in TFE (up) and in water (down) under the 365 nm UV lamp irradiation inside the camera obscura. (c) Fluorescence decays for BENI-COO⁻ (20 μM) and BENI-NH₃⁺ (20 μM) in TFE monitored at 470 nm and in H₂O monitored at 530 nm.

RESEARCH ARTICLE

fitted a monoexponential decay process (Figure 3c), indicating that the emission was resulted from the radiative geminate charge recombination. The fit results showed that the *J*-aggregates have a longer fluorescence lifetime (τ_f), as listed in Table S1 (See the Supporting Information). The fluorescence lifetime of BENI-NH₃⁺ aggregate was equal to 9.21 ns, longer than that (7.58 ns) of the BENI-COO⁻ counterparts. Interestingly, the BENI-NH₃⁺ aggregate gave a ϕ_F value of 11.8 %, which is ca. 5-fold larger than that (2.4 %) of the BENI-COO⁻ aggregate, suggesting that more amounts of long-lived CS states (separated electrons and holes) will be populated upon photoexcitation of the BENI-NH₃⁺ nanoribbons, benefiting probably the photoredox catalysis. This may be related to the intermolecular hydrogen bonds that led to the increased offset between the BENI chromophores in the extended short (*y*-axis) dimension. The electrochemical impedance spectroscopy of BENI-NH₃⁺ nanoribbons (Figure S5, See the Supporting Information) represented a smaller arc radius, indicating a stronger charge-transport ability, in agreement with the above-mentioned fluorescence results.

Ultrafast excited-state dynamics of BENI-COO⁻ and -NH₃⁺ monomers and aggregates. In order to gain more insight into the photophysical processes of photoexcited BENI-based monomers and aggregates, femtosecond transient absorption (fsTA) spectroscopy was used to study in detail the ultrafast exciton dynamics. Figure 4 showed the fsTA spectra of BENI-based monomers and aggregates. The similar excited-state absorptions (ESA) of the BENI-COO⁻ and -NH₃⁺ monomers indicated that the end substituents do not affect the excited-state dynamics of the individual BENI-based bolaamphiphiles (Figure 4a-b). The initial absorption spectra of monomers were comprised of the ground-state bleaching overlapped by simulated emission feature from 450 to 490 nm and the excited singlet state absorption band covering 490-740 nm. The severely broadened positive absorption clearly showed that the excited singlet state consisted of continuous manifold of vibrational levels. As the time evolution of the absorption, the spectra were gradually red-shifted, along with a decrease in intensity. The kinetic traces of BENI-COO⁻ and -NH₃⁺ monomers at 560 and 660 nm were shown in Figure S6 (See the Supporting Information), and the lifetimes were summarized in Table 1. The red-shift was resulted from the exothermic internal conversion (IC) from the initially-populated S_n state to the S₁ state in 3.0 ps (τ_1), and the vibrational relaxation of S₁ state in 40 ps (τ_2).^[15] The S₁ decay (S₁→S₀) was accompanied with the intersystem crossing, as a result, another positive and narrow absorption, which was ascribed to the lowest triplet states (T₁), gradually appeared at 660 nm.^[16] The T₁ state persisted across the entire time window, with the time constant of $\tau_5 \gg 6.0$ ns. The half-life of the S₁→T₁ decay component was 691 ± 25 ps (τ_4) for BENI-NH₃⁺, which was not determined accurately for BENI-COO⁻ due to the highly overlapping absorption features of S₁ and T₁. The lifetime of the S₁→S₀ decay component was 1.32 ± 0.15 ns (τ_3) for BENI-COO⁻ and 1.39 ± 0.17 ns (τ_3) for BENI-NH₃⁺, in consistent with their fluorescence lifetimes listed in Table S1.

The excited-state dynamics of BENI-COO⁻ and -NH₃⁺ aggregates are complicated by the presence of overlapping absorption bands of various origins, and consequently different from those of their monomers. The visible and near-infrared (NIR) fsTA spectra of BENI-COO⁻ and -NH₃⁺ aggregates in water under

400 nm laser excitation were shown in Figure 4c-d. It appeared that the initial ESA spectra of BENI-NH₃⁺ aggregate resembled that of BENI-COO⁻ aggregate. Besides a ground-state bleaching (GSB) below 450 nm, several positive absorption bands centered around 500, 630, 835 and 1300 nm were clearly discernable in the wide range of 450-1400 nm. These features all exhibited a multi-exponential decay, and the fit results of the fsTA data were listed in Table 1. The principal component at 835 nm should be attributed to the absorption of initial local (non-interacting) singlet excitons (S₁), because it raised first in < 200 fs (Figure 4e and f),^[17] followed by a fast relaxation decay in $\tau_1 = 0.61 \pm 0.05$ ps and the structural rearrangement in $\tau_2 = 8.14 \pm 1.1$ ps for BENI-COO⁻ aggregate. For the BENI-NH₃⁺ aggregate, the two processes proceeded in a several-fold time constant of $\tau_1 = 2.93 \pm 0.46$ ps and $\tau_2 = 90 \pm 15$ ps. Also, the lifetime of the S₁→S₀ exciton decay was 1.71 ± 0.21 ns, slower than that ($\tau_3 = 0.352 \pm 0.044$ ns) of the BENI-COO⁻ aggregate, indicating the stronger exciton delocalization. Following the S₁ exciton, the absorption band of subsequent transient species occurred at 500 nm, which could be assigned to the formation of Frenkel excitons (FEs, S₁S₀), which was resulted from the interaction between local excitations.^[14a, 18] The fit analysis of kinetic traces indicated a novel exciton decay pathway with a time constant of 0.99 ± 0.29 ps (τ_4) in the BENI-NH₃⁺ aggregate. To clarify the decay mechanism, we studied the excitation energy-dependence of ESA, as shown in Figure 4g and h. The excitation energy-dependent decay dynamics of FEs in BENI-COO⁻ aggregate was independent of the excitation power in subpicosecond time domain, whereas the BENI-NH₃⁺ aggregate showed a significant non-exponential decay of FEs, as a result of singlet-singlet or singlet-charge annihilation reactions (Figure S7, See the Supporting Information).^[17a, 19] This process took place when two excitons approached each other and their annihilation allowed an access to higher electronic states that have fast electronic relaxation channels.^[20] Accordingly, a fast decay in a lifetime (τ_4) of few ps was significantly observed in the ESA of BENI-NH₃⁺ aggregate. Despite the similarities in transient species of BENI-COO⁻ and -NH₃⁺ aggregates, the tremendous difference in decay dynamics of FEs may be related to the occurrence of hydrogen bonds, which led to the formation of BENI-NH₃⁺ nanoribbons. The intermolecular interaction facilitated the shuttle of FEs along the *y*-axis dimension of ribbon architectures.^[19]

Thereafter, the transient species at 1300 nm was pronounced in 2.0-10.0 ps (Figure 4e and f). It belonged to the charge-transfer (CT) state induced by the intermolecular electron/hole hopping (transfer) of FEs in the closely stacking BENI-based aggregates.^[21] The fit results showed that 56.6 % of CTEs have a longer lifetime (τ_3) of 4.22 ± 0.51 ns in the BENI-based aggregate, compared to the BENI-COO⁻ aggregate ($\tau_3 = 2.87 \pm 0.43$ ns, 10.4 %), responsible for the larger ϕ_F value (11.8 %). The formation of CTEs established the possibility of ultrafast charge separation, followed by the geminate charge recombination in a lifetime of 7.58 ns for the BENI-COO⁻ aggregate and 9.21 ns for the BENI-NH₃⁺ aggregate. The last one species appeared at 630 nm, which originated from the formation of mixed FE-CT excimers by hybridization between the FE and CTE due to the charge transfer equilibrium process.^[22] The schematic depiction of the exciton generation, separation and recombination processes occurring after photoexcitation of the BENI-based aggregates was displayed in Figure 4i.

RESEARCH ARTICLE

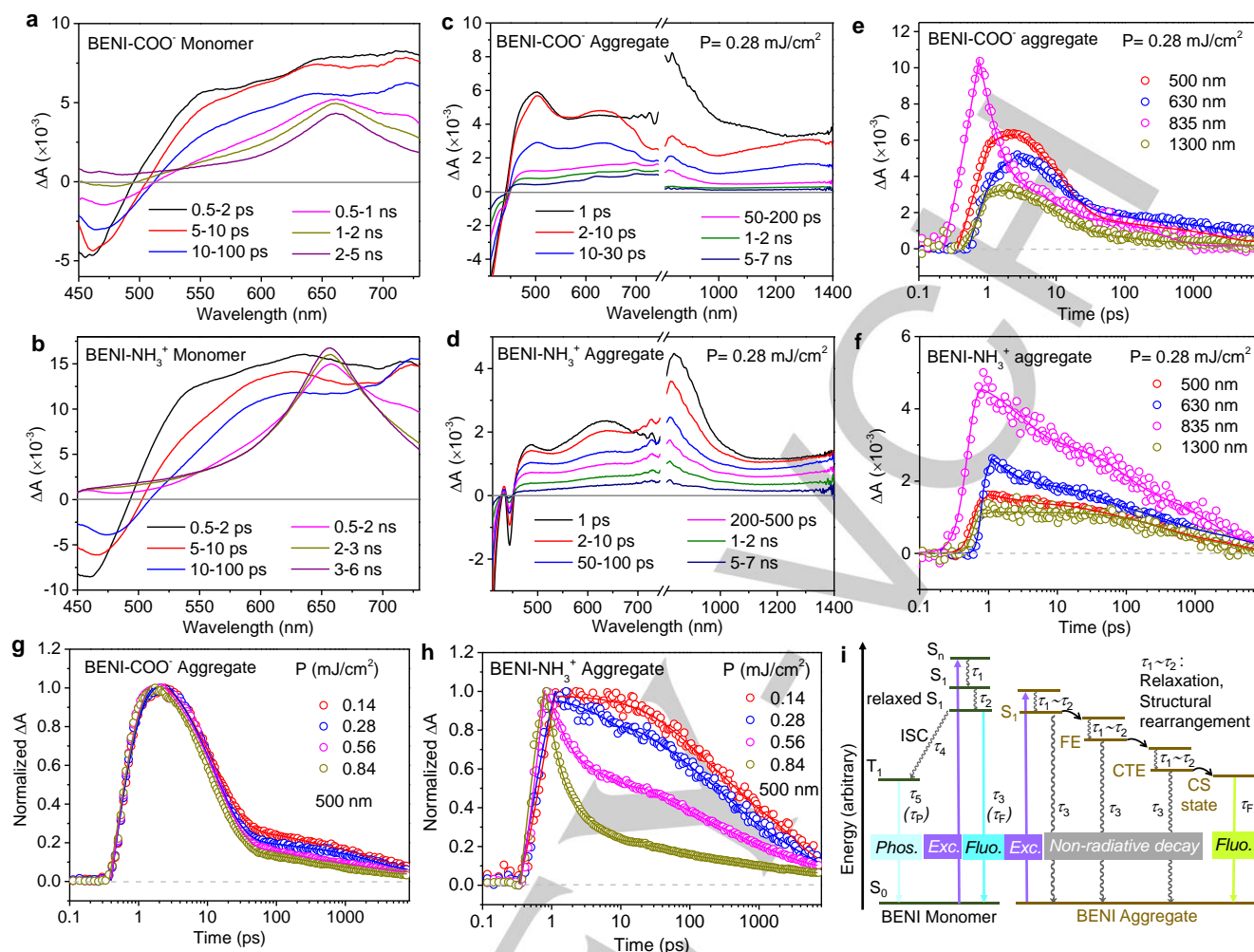


Figure 4. fsTA spectra of the BENI-COO⁻ (a) and BENI-NH₃⁺ (b) monomers in TFE under 380 nm laser excitation. The fsTA spectra of the BENI-COO⁻ (c) and BENI-NH₃⁺ (d) aggregates in H₂O under 400 nm laser excitation. Plots of kinetic traces of the BENI-COO⁻ (e) and BENI-NH₃⁺ (f) aggregates in H₂O probed at selected wavelengths (500, 630, 835 and 1300 nm). Excitation-energy-dependent dynamics of BENI-COO⁻ (g) and BENI-NH₃⁺ aggregates (h) in H₂O at 500 nm probe wavelength. (i) Schematic detailing of the relative energy levels and excited-state evolution for the BENI-COO⁻ and BENI-NH₃⁺ monomers and aggregates.

Table 1. Kinetic parameters of fsTA at low excitation density.

Molecule	Form	λ_{probe} (nm)	τ_1 (ps)	τ_2 (ps)	τ_3 (ns)	τ_4 (ps)	τ_5 (ns)
BENI-COO ⁻	Monomer	560	2.52 ± 0.23	44.5 ± 3.5	1.32 ± 0.15	–	–
		660	2.69 ± 0.16	47.5 ± 5.2	–	–	> 6.0
BENI-NH ₃ ⁺	Monomer	560	2.63 ± 0.02	37.6 ± 2.3	1.54 ± 0.17	–	–
		660	1.42 ± 0.27	24.7 ± 1.7	–	691 ± 25 ^[a]	> 6.0
BENI-COO ⁻	Aggregate	500	11.9 ± 0.2 (70.4 %)	108 ± 23 (10.3 %)	2.28 ± 0.28 (19.3 %)	–	–
		630	11.8 ± 0.4 (72.9 %)	96.0 ± 12.3 (12.4 %)	2.78 ± 0.23 (14.7 %)	–	–
		835	0.61 ± 0.05 (84.1 %)	8.14 ± 1.1 (9.96 %)	0.352 ± 0.044 (5.95 %)	–	–
		1300	12.2 ± 1.0 (67.4 %)	129 ± 28 (22.2 %)	2.87 ± 0.43 (10.4 %)	–	–
BENI-NH ₃ ⁺	Aggregate	500	42.0 ± 5.5 (17.5 %)	352 ± 47 (28.8 %)	3.71 ± 0.45 (25.9 %)	0.99 ± 0.29 ^[b] (27.8 %)	–
		630	40.0 ± 6.2 (17.9 %)	385 ± 57 (17.9 %)	4.51 ± 0.59 (15.9 %)	1.29 ± 0.28 ^[b] (48.4 %)	–
		835	2.93 ± 0.46 (38.9 %)	90 ± 15 (30.1 %)	1.71 ± 0.21 (31.0 %)	–	–
		1300	–	185 ± 34 (43.4 %)	4.22 ± 0.51 (56.6 %)	–	–

[a] The rising time constant of T₁ state. [b] The rate constant of exciton-exciton annihilation process.

RESEARCH ARTICLE

Electric field-mediated electron tunneling kinetics of BENI-based aggregates to atomic Ni center of DuBois Ni catalysts.

The above-mentioned *f*STA results indicated clearly that charge carriers were formed efficiently by photoexcitation of the BENI-based aggregates, in spite of no direct spectral evidences for the eventual formation of long-lived CS states. For the efficient extraction of hot charge carriers to drive photocatalytic redox reaction, two opposite-charged DuBois-Ni (Figure S1, See the Supporting Information) molecules as the electron collectors and hydrogen-evolving catalysts were designed and prepared to self-assemble electrostatically with the charged BENI-based aggregates to form the organic semiconductor-insulator-metal nanostructures (Figure S8, similar to BENI-based nanostructures, expect for the thicker layers ascribed to the electrostatically attracted DuBois-Ni), where an electrostatic field perpendicular to the BENI-based nanostructures can be formed (Figure 1). The change in fluorescence intensities of the two supramolecular MIS photosystems based on BENI-COO⁻ and -NH₃⁺ aggregates were studied in detail with increasing the concentration of DuBois Ni-NH₃⁺ and DuBois Ni-COO⁻, as shown in Figure 5a and b. From the slopes of the Stern-Volmer plots (Figure 5c, Table S2, See the Supporting Information), the bimolecular quenching constants (k_q) of BENI-COO⁻ and BENI-NH₃⁺ by Ni-NH₃⁺ and Ni-COO⁻ were calculated to be 1.61×10^{13} and 3.26×10^{12} M⁻¹ s⁻¹, respectively. Such k_q values were two or three orders of magnitude higher than the diffusion-controlled process (1.0×10^{10} M⁻¹ s⁻¹),^[23] indicating that the monomolecular (intramolecular) photochemical events did occur in the donor-acceptor supramolecular photosystems, BENI-COO⁻-NH₃⁺-Ni and BENI-NH₃⁺-COO⁻-Ni,^[24] instead of the bimolecular collisional quenching.

Figure 5d-f displayed the decay dynamics of the intramolecular photochemical process. They could be curve-fitted to be a bi-exponential function. The short lifetime was ascribed to the photo-induced electron transfer between donor and acceptor, while the

long-lived component was attributed to the emission of BENI-COO⁻ or -NH₃⁺ aggregates. The rate constant of electron transfer (k_{ET}) was evaluated according to the Equation ($k_{ET} = (1/\tau)_{\text{sample}} - (1/\tau)_{\text{ref}}$) in the usual process.^[24-25] The measured k_{ET} values were summarized in Table S3 (See the Supporting Information). The rate constant of electron transfer within BENI-COO⁻-NH₃⁺-Ni was considerably faster than that of BENI-NH₃⁺-COO⁻-Ni (Figure 5f). The large difference revealed that the electron transfer in the supramolecular MIS photosystems was mediated by the salt bridge, similar with the biological environment of proteins and enzymes, where the internal EF affected the rate of electron transfer.^[26] In the BENI-COO⁻-NH₃⁺-Ni photosystem, the permanent dipole ($\delta^- \delta^+$) of the salt bridge (COO⁻-NH₃⁺) was in line with the electron transfer direction, whereas in the BENI-NH₃⁺-COO⁻ photosystem the permanent dipole ($\delta^+ \delta^-$) of the salt bridge (NH₃⁺-COO⁻) opposed the electron transfer. In addition, the rate constant (k_{ET}) of electron transfer increased linearly with increasing the concentration of charged DuBois Ni catalysts. This is mainly because each BENI-based bolaamphiphilic monomer has two charged hydrophilic head-groups, while each DuBois Ni catalyst is composed of four opposite charged hydrophilic head-groups. As a result, the composition and structure of supramolecular MIS photosystems can be tuned by altering the ratio of DuBois Ni catalysts to bolaamphiphilic chromophores (Figure S9-10, See the Supporting Information). Significantly, more amounts of salt bridges formed between the bolaamphiphilic donors and the Ni acceptors improved the electron transfer rate. When the molar ratio of the DuBois Ni catalyst to the bolaamphiphilic chromophore was equal to 0.37, the rate constants of electron transfer (k_{ET}) were determined to be 6.12×10^8 s⁻¹ for BENI-COO⁻-NH₃⁺-Ni and 1.17×10^8 s⁻¹ for BENI-NH₃⁺-COO⁻-Ni, respectively. The former is 5-fold larger than the latter, corresponding to the efficiency of electron tunneling to the atomic Ni sites across the long-distance alkyl region and a salt

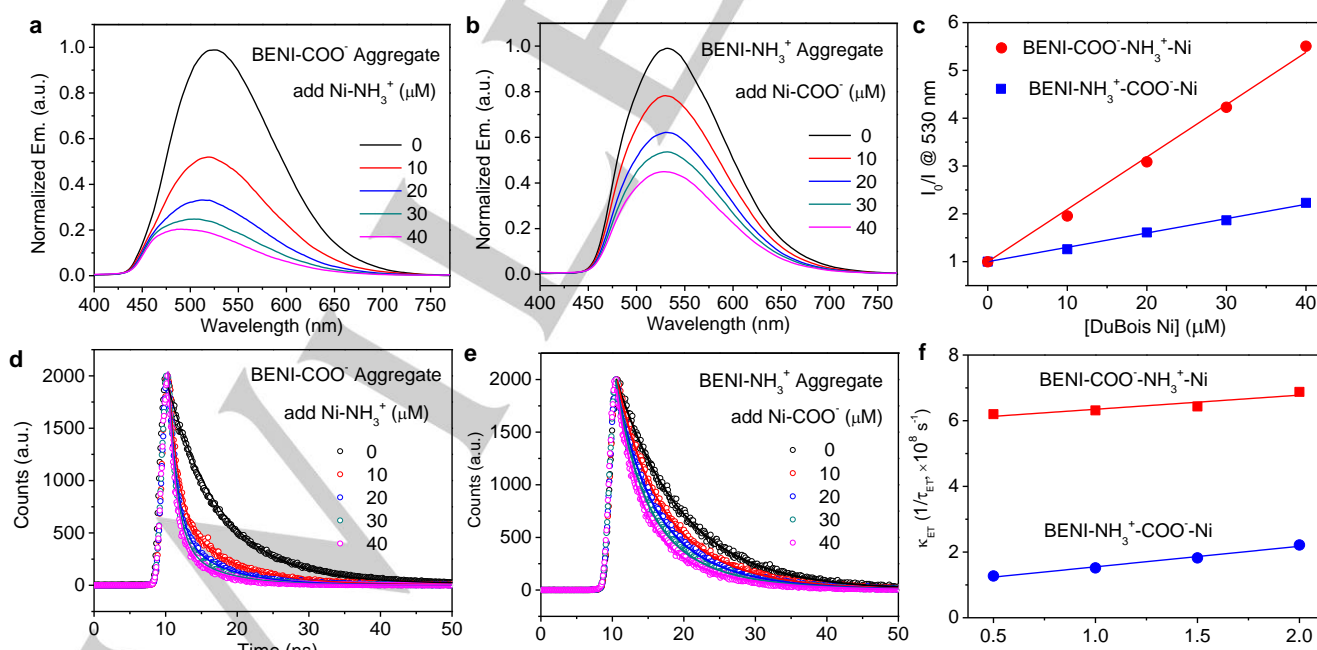


Figure 5. Fluorescence emission spectra of the BENI-COO⁻ (a) and BENI-NH₃⁺ (b) (20 μM) with the increasing addition of DuBois Ni-NH₃⁺ and Ni-COO⁻ (0-40 μM) in water. (c) Stern-Volmer plots for the fluorescence intensity monitored at 530 nm. I_0 is the initial fluorescence intensity, I is the fluorescence intensity at the corresponding concentration of DuBois Ni-COO⁻ (or Ni-NH₃⁺). Time-resolved fluorescence decays monitored at 530 nm of the BENI-COO⁻ (d) and BENI-NH₃⁺ (e) (20 μM) with the increasing addition of DuBois Ni-NH₃⁺ and Ni-COO⁻ (0-40 μM) in water. (f) Plot of the rate constant (k_{ET}) for electron transfer from BENI-based aggregates to the opposite-charged DuBois-Ni catalyst with different molar ratios. Excited at 390 nm.

RESEARCH ARTICLE

bridge interface. Obviously, both of the electron tunneling rate (ETR) and the fluorescence quantum yield (FQY) resulted from the geminate charge recombination are the most crucial parameters determining the overall efficiency of the supramolecular MIS photosystems for biomimetic hydrogen production.

Supramolecular BENI-COO⁻-NH₃⁺-Ni and BENI-NH₃⁺-COO⁻-Ni MIS photosystems for biomimetic hydrogen production.

The photocatalytic H₂-evolution activities of the biomimetic supramolecular photosystems were evaluated using ascorbic acid (H₂A) as a sacrificial electron donor under visible-light ($\lambda \geq 400$ nm) at pH = 4, after the optimization of reaction conditions (Figure S11, See the Supporting Information). A set of control experiments were carried out in the absence of BENI-COO⁻ (or BENI-NH₃⁺) or DuBois Ni-NH₃⁺ (or Ni-COO⁻) or ascorbic acid or light. Either trace amount of H₂, or no H₂ was detected by GC (Figure 6a), indicating that all components are prerequisite for the photocatalytic hydrogen production. The time-dependent hydrogen evolution of BENI-COO⁻-NH₃⁺-Ni and BENI-NH₃⁺-COO⁻-Ni photosystems was shown in Figure 6b. The average hydrogen evolution rate for BENI-COO⁻-NH₃⁺-Ni and BENI-NH₃⁺-COO⁻-Ni reached, respectively, up to 3.25 and 2.71 mmol·g⁻¹·h⁻¹ under irradiation of first 3 h. However, both of them decreased significantly after irradiation of > 4 h and the H₂ production stopped after about 10 h (Figure 6b). It indicated the degradation of at least one component in the photosystems. If the same quantity of fresh BENI-COO⁻ (or BENI-NH₃⁺) or H₂A was re-added to the inactive solution, H₂ production cannot be activated again. Nevertheless, the reactivation was observed upon re-adding the same quantity of fresh DuBois Ni-NH₃⁺ (or Ni-COO⁻) catalysts. A repeating pattern of resumed activity followed by gradual decay of the DuBois Ni catalysts occurred (Figure S12, See the Supporting Information), consistent with the previous reports for short lifetime of these DuBois Ni catalysts in photocatalytic

systems.^[27] Moreover, the rate of photocatalytic H₂ production in our systems with the re-added molecular Ni catalysts was much lower than the fresh one. This is mainly originated from the outer coordination sphere of the decayed DuBois Ni catalysts survived on the surface of BENI-based nanostructures (Figure S12, See the Supporting Information), which impeded the electrostatic assembly of fresh molecular Ni catalysts with the BENI-based semiconductors to regenerate MIS-type photosystems. Although no any discernible changes of functional groups and morphologies were observed for the BENI-COO⁻-NH₃⁺-Ni and BENI-NH₃⁺-COO⁻-Ni photosystems after 10 h illumination (Figure S13-S14, See the Supporting Information), their crystallinities became slightly weaker (Figure S15, See the Supporting Information). It might not be benefit for the charge separation. To improve the long-term stability of the biomimetic photocatalysts, more stable molecular catalysts could be used, for example, CoPc,^[28] [Ni(DHMPE)₂]²⁺,^[29] and so on.

Next, we examined the dependence of apparent quantum efficiency (AQE) on the wavelength of incident light. It appeared in Figure 6c that the AQE values matched well with their optical absorptions, proving that the reaction was a light-driven redox process. The largest quantum efficiency of 1.63 % for BENI-COO⁻-NH₃⁺-Ni and 1.51 % for BENI-NH₃⁺-COO⁻-Ni were achieved at 400 nm, respectively, further confirming that the equal contribution of the two elementary steps, charge separation and interfacial transfer, to the redox photocatalysis. The electrochemical analysis results showed that the BENI-COO⁻ and -NH₃⁺ aggregates had the equivalent flat band potentials of -1.03 ~ -1.11 V vs. RHE (Figure S16, See the Supporting Information), more negative than that (-0.21 V vs. RHE) of the DuBois Ni catalysts.^[27b] Their valence band (VB) potentials were more positive than the oxidation potential of H₂A (+0.41 V vs. RHE).^[30] The results indicated that oxidative and reductive quenching of excitons in the photoexcited BENI-based aggregates were both

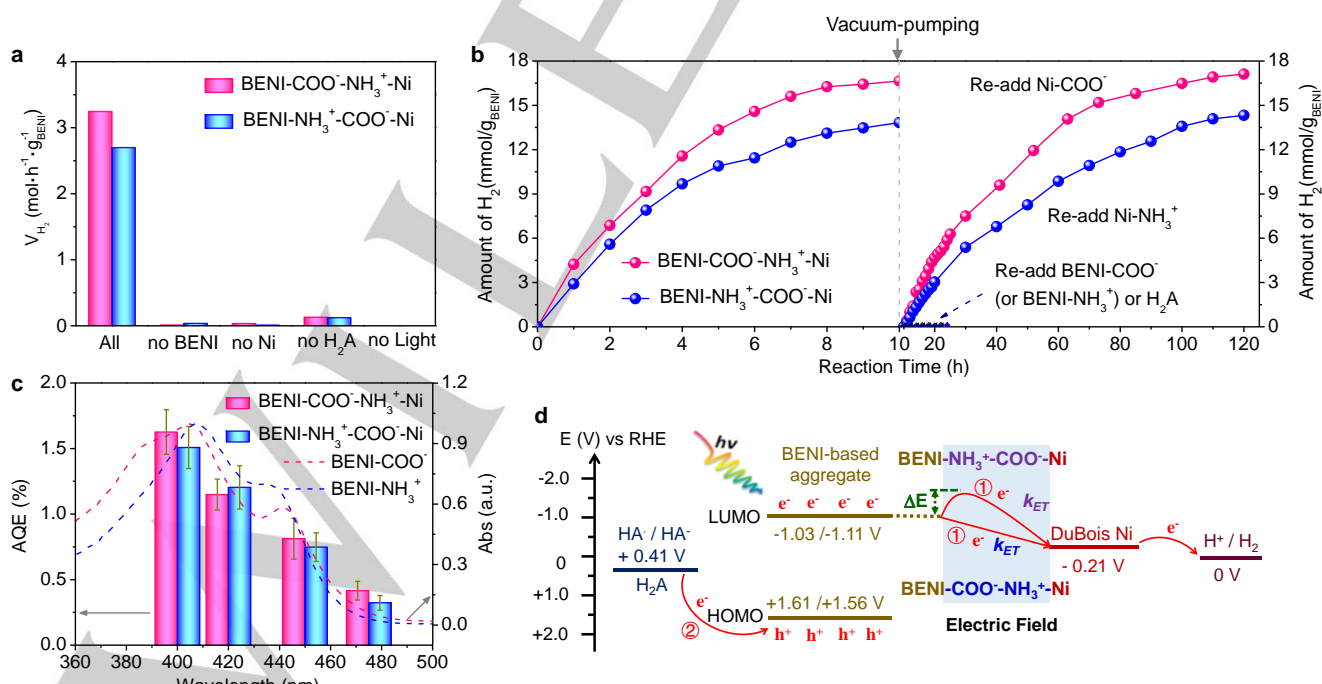


Figure 6. (a) Photocatalytic H₂ production rates of BENI-COO⁻-NH₃⁺-Ni and BENI-NH₃⁺-COO⁻-Ni biomimetic photosystems in the presence of ascorbic acid (H₂A) as electron donor during the initial 3 h under visible light irradiation ($\lambda \geq 400$ nm) at pH 4. (b) Time course of hydrogen evolution of BENI-COO⁻-NH₃⁺-Ni and BENI-NH₃⁺-COO⁻-Ni MIS photosystems. (c) The action spectra of BENI-COO⁻-NH₃⁺-Ni and BENI-NH₃⁺-COO⁻-Ni biomimetic photosystems for H₂ production. (d) Proposed photocatalytic mechanism of supramolecular MIS biomimetic photosystems and the electric field-mediated redox chemistry for hydrogen production

RESEARCH ARTICLE

thermodynamically favorable. Interestingly, adding H₂A, the fluorescence quenching of BENI-based aggregates was very weak (Figure S17, See the supporting materials), suggesting that the long-distance tunneling of photo-induced electrons from the excited BENI-based aggregates to the atomic Ni centers initiated the photocatalytic process, followed by the one-hole oxidation of H₂A to release protons (Figure 6d). In a word, the organic semiconductor photocatalysis involved mainly the oxidative quenching mechanism of excitons and the electron tunneling separation highly sensitive for the electric field.

Conclusion

Two supramolecular BENI-COO⁻-NH₃⁺-Ni and BENI-NH₃⁺-COO⁻-Ni photosystems were constructed by integrating novel charged BENI-based bolaamphiphiles (BENI-COO⁻ and BENI-NH₃⁺) with opposite-charged Ni catalysts in water. The electric field formed by the slat bridges played an important role as an electron-tunneling mediator in the electron-transfer reaction. In the present of ascorbic acid as electron donors in water, these two supramolecular MIS photosystems gave a H₂ evolution rate of 3.25 mmol·g⁻¹·h⁻¹ for BENI-COO⁻-NH₃⁺-Ni and 2.71 mmol·g⁻¹·h⁻¹ for BENI-NH₃⁺-COO⁻-Ni under visible light irradiation, corresponding to the AQEs at 400 nm of 1.63 % and 1.52 %, respectively. The time-resolved spectral studies revealed the decay trajectory of excitons in the self-assembled nanostructures, undergoing from singlet state, to Frenkel state, to CT state, and finally to CS state with a half-life of 7.58 ns for BENI-COO⁻ and 9.21 ns for BENI-NH₃⁺. The hydrogen bonds in BENI-NH₃⁺ aggregates benefited the formation long-lived CS states, which caused a higher ϕ_F value of 11.8 %. The rate of electron tunneling to the atomic Ni sites across the long-distance alkyl region and a salt bridge interface was determined to be 6.12×10^8 s⁻¹ for BENI-COO⁻-NH₃⁺-Ni, which is ca. 5-fold larger than that (1.17×10^8 s⁻¹) of BENI-NH₃⁺-COO⁻-Ni, whereas the ϕ_F value of the former is ca. 5-fold less than the latter. Both of charge-separation and electron tunneling rates are the most crucial parameters determining the overall efficiency of biomimetic hydrogen production. This work offered a conceptual guidance for design and synthesis of small-molecule organic semiconductors with negative charges to fabricate MIS-type photosystems with more stable molecular catalysts for high-performance, stable, and biomimetic hydrogen production.

Acknowledgements

The NSFC (Grants No. 22072022, 21773031), National Key R&D Program of China (2018YFE0208500), the Natural Science Foundation of Fujian Province of P. R. China (2018J01686), and the State Key Laboratory of Photocatalysis on Energy and Environment (SKLPEE-2017A01 and SKLPEE-2017B02) financially supported this work.

Keywords: Biomimetic Photocatalysis • Electron Tunneling • Molecular Semiconductor • H₂ production • Naphthalimide • MIS Heterojunction

- [1] a) R. S. Sprick, J.-X. Jiang, B. Bonillo, S. Ren, T. Ratvijitvech, P. Guiglion, M. A. Zwijnenburg, D. J. Adams, A. I. Cooper, *J. Am. Chem. Soc.* **2015**, *137*, 3265–3270; b) G. Zhang, Z. A. Lan, X. Wang, *Angew. Chem. Int. Ed.* **2016**, *55*, 15712–15727; *Angew. Chem.* **2016**, *128*, 15940–15956; c) T. Banerjee, K. Gottschling, G. Savaschi, C. Ochsenfeld, B. V. Lotsch, *ACS Energy Lett.* **2018**, *3*, 400–409; d) Y. Zhao, H. Liu, C. Wu, Z. Zhang, Q. Pan, F. Hu, R. Wang, P. Li, X. Huang, Z. Li, *Angew. Chem. Int. Ed.* **2019**, *58*, 5376–5381; *Angew. Chem.* **2019**, *131*, 5430–5435; e) J. Ming, A. Liu, J. Zhao, P. Zhang, H. Huang, H. Lin, Z. Xu, X. Zhang, X. Wang, J. Hofkens, M. B. J. Roeffaers, J. Long, *Angew. Chem. Int. Ed.* **2019**, *58*, 18290–18294. *Angew. Chem.* **2019**, *131*, 18458–18462. f) C. Dai, B. Liu, *Energy Environ. Sci.* **2020**, *13*, 24–52.
- [2] a) A. S. Weingarten, R. V. Kazantsev, L. C. Palmer, M. McClendon, A. R. Koltonow, A. P. Samuel, D. J. Kiebal, M. R. Wasielewski, S. I. Stupp, *Nat. Chem.* **2014**, *6*, 964–970; b) A. S. Weingarten, A. J. Dannenhoffer, R. V. Kazantsev, H. Sai, D. Huang, S. I. Stupp, *J. Am. Chem. Soc.* **2018**, *140*, 4965–4968.
- [3] a) M. Knupfer, *Appl. Phys. A* **2003**, *77*, 623–626; b) P. K. Nayak, *Synth. Met.* **2013**, *174*, 42–45; c) M. Muntwiler, Q. Yang, W. A. Tisdale, X.-Y. Zhu, *Phys. Rev. Lett.* **2008**, *101*, 196403; d) V. Arkhipov, H. Bässler, *Phys. Status Solidi A* **2004**, *201*, 1152–1187.
- [4] a) L. Wang, W. Huang, R. Li, D. Gehrig, P. W. Blom, K. Landfester, K. A. Zhang, *Angew. Chem. Int. Ed.* **2016**, *55*, 9783–9787; *Angew. Chem.* **2016**, *128*, 9935–9940; b) D. Liu, J. Wang, X. Bai, R. Zong, Y. Zhu, *Adv. Mater.* **2016**, *28*, 7284–7290; c) R. V. Kazantsev, A. J. Dannenhoffer, T. Aytun, B. Harutyunyan, D. J. Fairfield, M. J. Bedzyk, S. I. Stupp, *Chem* **2018**, *4*, 1596–1608.
- [5] a) S. V. Bhosale, C. H. Jani, S. J. Langford, *Chem. Soc. Rev.* **2008**, *37*, 331–342; b) M. Avinash, T. Govindaraju, *Adv. Mater.* **2012**, *24*, 3905–3922.
- [6] a) M. R. Molla, S. Ghosh, *Chem. Mater.* **2010**, *23*, 95–105; b) H. Katz, A. Lovinger, J. Johnson, C. Kloc, T. Siegrist, W. Li, Y.-Y. Lin, A. Dodabalapur, *Nature* **2000**, *404*, 478–481.
- [7] N. Sakai, J. Mareda, E. Vauthey, S. Matile, *Chem. Commun.* **2010**, *46*, 4225–4237.
- [8] a) V. Lin, S. G. DiMaggio, M. J. Therien, *Science* **1994**, *264*, 1105–1111; b) J. Chen, J. Xi, D. Wang, Z. Shuai, *J. Phys. Chem. Lett.* **2013**, *4*, 1443–1448; c) P. Pachfule, A. Acharya, J. r. m. Roeser, T. Langenhahn, M. Schwarze, R. Schomäcker, A. Thomas, J. Schmidt, *J. Am. Chem. Soc.* **2018**, *140*, 1423–1427.
- [9] C. Wang, Z. Wang, X. Zhang, *Acc. Chem. Res.* **2012**, *45*, 608–618.
- [10] a) A. Le Goff, V. Artero, B. Jusselme, P. D. Tran, N. Guillet, R. Métayé, A. Fihri, S. Palacin, M. Fontecave, *Science* **2009**, *326*, 1384–1387; b) A. D. Wilson, R. K. Shoemaker, A. Miedaner, J. T. Muckerman, D. L. DuBois, M. R. DuBois, *Proc. Nat. Acad. Sci.* **2007**, *104*, 6951–6956.
- [11] T. Seki, Y. Maruya, K.-i. Nakayama, T. Karatsu, A. Kitamura, S. Yagai, *Chem. Commun.* **2011**, *47*, 12447–12449.
- [12] a) Y. Liu, H. Wang, G. Chen, X. Xu, S. Ji, *Aust. J. Chem.* **2009**, *62*, 934–940; b) X. Cao, L. Meng, Z. Li, Y. Mao, H. Lan, L. Chen, Y. Fan, T. Yi, *Langmuir* **2014**, *30*, 11753–11760.
- [13] Z. Yu, Y. Wu, Q. Liao, H. Zhang, S. Bai, H. Li, Z. Xu, C. Sun, X. Wang, J. Yao, *J. Am. Chem. Soc.* **2015**, *137*, 15105–15111.
- [14] a) N. J. Hestand, F. C. Spano, *Acc. Chem. Res.* **2017**, *50*, 341–350; b) M. Kirkus, L. Wang, S. Mothy, D. Beljonne, J. Cornil, R. A. Janssen, S. C. Meskers, *J. Phys. Chem. A* **2012**, *116*, 7927–7936.
- [15] P. Kucheryavy, G. Li, S. Vyas, C. Hadad, K. D. Glusac, *J. Phys. Chem. A* **2009**, *113*, 6453–6461.
- [16] A. Samanta, B. Ramachandram, G. Saroja, *J. Photochem. Photobiol., A* **1996**, *101*, 29–32.
- [17] a) J. M. Lim, P. Kim, M.-C. Yoon, J. Sung, V. Dehm, Z. Chen, F. Würthner, D. Kim, *Chem. Sci.* **2013**, *4*, 388–397; b) N. Banerji, S. Cowan, M. Leclerc, E. Vauthey, A. J. Heeger, *J. Am. Chem. Soc.* **2010**, *132*, 17459–17470.
- [18] M. Hoffmann, K. Schmidt, T. Fritz, T. Hasche, V. M. Agranovich, K. Leo, *Chem. Phys.* **2000**, *258*, 73–96.
- [19] A. C. Jakowetz, T. F. Hinrichsen, L. Ascherl, T. Sick, M. Calik, F. Auras, D. D. Medina, R. H. Friend, A. Rao, T. Bein, *J. Am. Chem. Soc.* **2019**, *141*, 11565–11571.
- [20] G. Soavi, S. Dal Conte, C. Manzoni, D. Viola, A. Narita, Y. Hu, X. Feng, U. Hohenester, E. Molinari, D. Prezzi, *Nat. Commun.* **2016**, *7*, 11010.

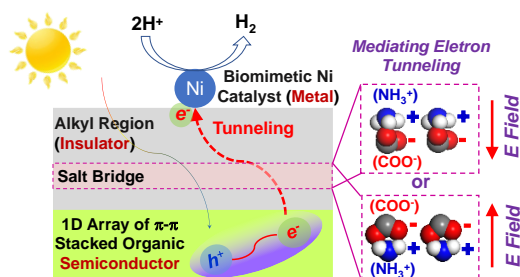
RESEARCH ARTICLE

- [21] E. A. Margulies, L. E. Shoer, S. W. Eaton, M. R. Wasielewski, *Phys. Chem. Chem. Phys.* **2014**, *16*, 23735-23742.
- [22] a) R. Katoh, E. Katoh, N. Nakashima, M. Yuuki, M. Kotani, *J. Phys. Chem. A* **1997**, *101*, 7725-7728; b) R. E. Cook, B. T. Phelan, R. J. Kamire, M. B. Majewski, R. M. Young, M. R. Wasielewski, *J. Phys. Chem. A* **2017**, *121*, 1607-1615.
- [23] K. C. Chou, G. P. Zhou, *J. Am. Chem. Soc.* **1982**, *104*, 1409-1413.
- [24] M. E. El - Khouly, L. M. Rogers, M. E. Zandler, G. Suresh, M. Fujitsuka, O. Ito, F. D'Souza, *ChemPhysChem* **2003**, *4*, 474-481.
- [25] A. N. Macpherson, P. A. Liddell, S. Lin, L. Noss, G. R. Seely, J. M. DeGraziano, A. L. Moore, T. A. Moore, D. Gust, *J. Am. Chem. Soc.* **1995**, *117*, 7202-7212.
- [26] J. P. Kirby, J. A. Roberts, D. G. Nocera, *J. Am. Chem. Soc.* **1997**, *119*, 9230-9236.
- [27] a) B. C. Martindale, G. A. Hutton, C. A. Caputo, E. Reisner, *J. Am. Chem. Soc.* **2015**, *137*, 6018-6025; b) M. A. Gross, A. Reynal, J. R. Durrant, E. Reisner, *J. Am. Chem. Soc.* **2013**, *136*, 356-366; c) C. A. Caputo, M. A. Gross, V. W. Lau, C. Cavazza, B. V. Lotsch, E. Reisner, *Angew. Chem.* **2014**, *126*, 11722-11726.
- [28] a) S. Ren, D. Joulié, D. Salvatore, K. Torbensen, M. Wang, M. Robert, C. P. Berlinguette, *Science* **2019**, *365*, 367-369; b) Y. Wu, Z. Jiang, X. Lu, Y. Liang, H. Wang, *Nature* **2019**, *575*, 639-642.
- [29] C. Tsay, J. Y. Yang, *J. Am. Chem. Soc.* **2016**, *138*, 14174-14177.
- [30] N. H. Williams, J. K. Yandell, *Aust. J. Chem.* **1982**, *35*, 1133-1144.

RESEARCH ARTICLE

Entry for the Table of Contents

Insert graphic for Table of Contents here.



Electric field mediated photoredox chemistry. Two charged organic semiconductors based on naphthalimide bolaamphiphiles were designed to fabricate metal-insulator-semiconductor (MIS) photosystems with opposite-charged DuBois nickel catalysts for biomimetic H₂ evolution. The photo-induced charge carriers can be efficiently separated and tunneled to the Ni collectors across salt bridges and alkyl regions to reduce protons to H₂, which mediated by the intermolecular electrostatic field.